Letter

Non-Hermitian edge burst without skin localization

C. Yuce [1] and H. Ramezani [2]

[1]*Department of Physics, Eskisehir Technical University, Eskisehir 26555, Turkey*

[2]*Department of Physics and Astronomy, University of Texas Rio Grande Valley, Edinburg, Texas 78539, USA*

(Received 15 November 2022; revised 22 March 2023; accepted 27 March 2023; published 13 April 2023)

In a class of non-Hermitian quantum walk in lossy lattices with open boundary conditions, an unexpected peak in the distribution of the decay probabilities appears at the edge, referred to as an edge burst. It is proposed that the edge burst originates jointly from the non-Hermitian skin effect (NHSE) and the imaginary gaplessness of the spectrum [W.-T. Xue *et al.*, Phys. Rev. Lett. **128**, 120401 (2022)]. Using a particular one-dimensional lossy lattice with a nonuniform loss rate, we show that the edge burst can occur even in the absence of skin localizations. Furthermore, we discuss that the edge burst may not appear if the spectrum satisfies the imaginary gapless condition. Aside from its fundamental importance, by removing the restrictions on observing the edge burst effect, our results open the door to broader design space for future applications of the edge burst effect.

DOI: 10.1103/PhysRevB.107.L140302

Introduction. The past two decades have witnessed an abundance of promising work in extending the quantum theory to the non-Hermitian domain. Among the many fascinating aspects of non-Hermitian Hamiltonians, the non-Hermitian skin effect (NHSE) has recently attracted a great deal of attention [1,2]. The NHSE implies that the complex spectrum of a non-Hermitian lattice can be highly sensitive to the boundary conditions, and the eigenstates that are not at the Bloch points (at which the eigenvalues are the same under periodic and open boundary conditions) are localized at the edge of the open lattice [3–31]. The non-Bloch band theory has been formulated to explain the intriguing features of the NHSE [32]. The NHSE and topology are interconnected [33–38], and the NHSE can thus be predicted using the spectral winding number [33].

Quantum dynamics in non-Hermitian systems are believed to be quite different from standard Hermitian systems. The quantum walk that was originated from a generalization of the classical random walk has also been extended to non-Hermitian systems [39]. A quantum walker will completely leak out eventually from a bipartite lossy lattice with uniform loss rates [40]. The quantum walker in this system is expected to escape predominantly from nearby sites of a starting point that is far from the edges. However, numerical computations show that the decay probability distribution is left-right asymmetric, and a relatively large peak in the loss probability at the farthest edge from the starting point occurs. More unexpectedly, the relative height of this peak grows with the distance between the starting point and the edge. Originally, it was attributed to topological edge states [40], which was questioned in a recent paper [41]. The appearance of an edge peak (a so-called edge burst) was demonstrated to stem entirely from the interplay between two prominent non-Hermitian phenomena, the NHSE and imaginary gap closing [41]. The left-right asymmetry is attributed to the NHSE since all eigenstates are localized at one edge of the system, and the large peak at the edge is due to the imaginary gap closing.

In this Letter, we show that an edge burst can occur even in the absence of skin localizations. We consider the same lattice as Refs. [40,41] but with nonuniform loss rates. The NHSE disappears due to the nonuniform nature of the loss rates, but the imaginary gap closing condition on the spectrum is satisfied. The left-right asymmetry of the decay probability occurs in the system due to the phase difference of the couplings in each unit cell. We also demonstrate that there exist systems with a left-right asymmetric decay probability and without an edge burst even if the imaginary gap closing condition on the spectrum is satisfied.

Quantum walk. We consider a quantum walker in a tight-binding one-dimensional non-Hermitian lattice with N unit cells. The lattice as shown in Fig. 1 is composed of two sublattices $\mathcal{A}$ and $\mathcal{B}$. The non-Hermiticity comes from the lossy $\mathcal{B}$ sublattice with nonuniform loss rates. The dynamics of the quantum walker in this lattice obeys the following coupled equations,

$$\begin{aligned} i\frac{d\psi_n^A}{dt} &= t_1\psi_n^B + i\frac{t_2}{2}\left(\psi_{n-1}^A - \psi_{n+1}^A\right) + \frac{t_2}{2}\left(\psi_{n-1}^B + \psi_{n+1}^B\right) \\ i\frac{d\psi_n^B}{dt} &= t_1\psi_n^A - i\frac{t_2}{2}\left(\psi_{n-1}^B - \psi_{n+1}^B\right) + \frac{t_2}{2}\left(\psi_{n-1}^A + \psi_{n+1}^A\right) \\ &\quad -i\,\gamma_n\,\psi_n^B\,, \end{aligned} \tag{1}$$

where $n = 1, 2, \ldots, N$, $\psi_n^A(t)$ and $\psi_n^B(t)$ are time-dependent complex field amplitudes in the $\mathcal{A}$ and $\mathcal{B}$ sublattices, respectively, t_1 and t_2 are real positive parameters describing couplings, and $\gamma_n > 0$ are site-dependent loss rates.

Suppose that the quantum walker is initially placed in the $\mathcal{A}$ sublattice at the starting unit cell S that is supposed to be close to the right edge. Therefore, the initial conditions are given by $\psi_n^A(t=0) = \delta_{n,S}$ and $\psi_n^B(t=0) = 0$. To study the dynamics, we numerically solve Eq. (1) subject to the open boundary conditions and the above initial conditions. During the quantum walk, the walker moves in discrete steps in both sublattices and escapes only from lossy $\mathcal{B}$ sites. As $t \to \infty$, the walker completely leaks out from the system. The decay

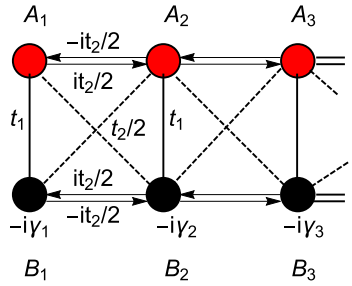

FIG. 1. The lossy finite tight-binding lattice with two sublattices. Losses occur only in the $\mathcal{B}$ sublattice with nonuniform loss rates $\gamma_n = \{\gamma_1, \gamma_2, \ldots, \gamma_N\}$ with N being the total number of unit cells. A quantum walker starts in the $\mathcal{A}$ sublattice A_S that is supposed to be close to the right edge. As $t \to \infty$, the walker completely leaks out from the system.

probability that the quantum walker escapes from the leaky $\mathcal{B}$ sublattice with the site number n is given by [40]

$$P_n = 2\,\gamma_n \int_0^\infty \left|\psi_n^B(t)\right|^2 dt, \tag{2}$$

with total decay probability conservation $\sum_{n=1}^{N} P_n = 1$.

As a special case, the system exhibits left-right asymmetry in decay probabilities when the loss rate is uniform ($\gamma_n = \gamma$) [40,41]. In this case, P_n is maximum at $n = S$ and decreases algebraically in the bulk as n decreases from S, and then makes a sharp peak at the left edge (edge burst). On the other hand, P_n is very small for $n > S$. We are interested in exploring the edge burst for a system with nonuniform loss rates. We think that we can enhance or suppress the edge burst by a proper choice of γ_n. For example, one intuitively expects that it can be suppressed if γ_n are large around the starting point S but small around the left edge. Let us specifically suppose that the loss rate increases linearly from the left edge with a constant rate of change γ,

$$\gamma_n = \gamma\, n, \tag{3}$$

from which one may naively say that the edge burst can be suppressed by thinking that the quantum walker escapes from the system before reaching the left edge of the lattice ($N \gg 1$ and $S \gg 1$). But we numerically see that this is not the case. In fact, the system has radically different behavior from its uniformly lossy analog and the edge burst can be enhanced instead.

To quantify the edge burst, we use the relative height, defined as $P_1/P_{\min}$, where $P_{\min} = \min\{P_1, P_2, \ldots, P_S\}$ is the minimum of P_n between the left edge and the starting point S. We note that $P_1/P_{\min} \gg 1$ and $P_1/P_{\min} \sim 1$ are evidence of the existence and absence of the edge burst, respectively [41]. We can also define another ratio P_1/P_S to compare the decay probabilities at the left edge and starting point. For the uniform loss rate, this ratio is always smaller than 1, indicating that the quantum walker leaks out more from the starting unit cell than the one at the left edge [Fig. 2(a)]. However, the ratio P_1/P_S can be bigger than 1 for the nonuniform loss rate (3) as can be seen from Figs. 2(b)–2(d). This is counterintuitive as it is natural to expect the quantum walker to decay mostly from the starting unit cell, and not from the farthest unit cell,

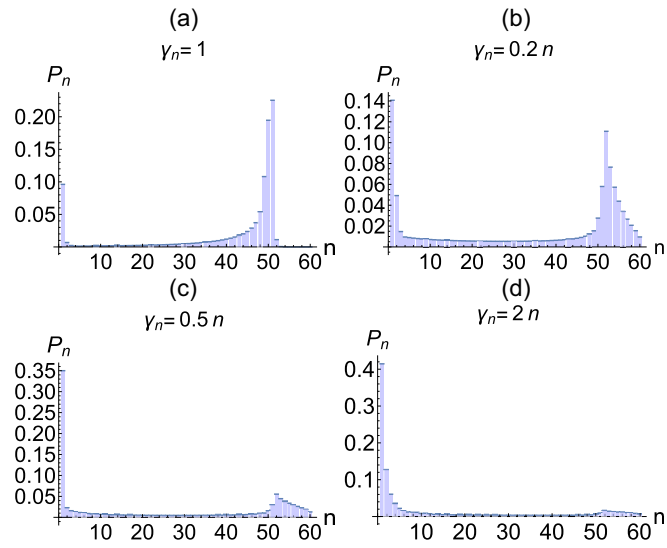

FIG. 2. The distribution of the decay probabilities for the (a) uniform and (b)–(d) nonuniform loss rates. The ratio $\frac{P_1}{P_{\min}}$ is bigger than one for all figures [18, 25, 76, and 124 for (a)–(d), respectively]. However, the ratio $\frac{P_1}{P_S}$ is smaller than 1 only for (a). The edge burst is enhanced with increasing γ: 14%, 35%, and 40% of the total decay occur at the left edge for (b), (c), and (d), respectively. Skin localizations are absent in (b)–(d), hence the left-right asymmetry in (b)–(d) cannot be attributed to the NHSE. The decay probabilities do not fall sharply to the right of the starting point in (b)–(d) as opposed to the case in (a). The parameters are $t_1 = 0.3$, $t_2 = 0.5$, $S = 50$, and $N = 60$.

which also has the least loss rate. It seems that the quantum walker reaches the left edge with less losses if we increase γ and waits there until it decays completely from there. We find that P_1 grows with γ, whereas P_S decreases with it. At quite large values of the loss rate ($\gamma > 3$), the peak at the starting point disappears. We can also compare the behavior of P_n in the bulk with $S > n > 1$. P_n decreases algebraically in the bulk as n decreases from S when the loss rate is uniform, $\gamma_n = \gamma$ [Fig. 2(a)]. However, it stays almost constant at many sites in the bulk when the loss rate is nonuniform (3) [Figs. 2(b)–2(d)]. In each plot in Fig. 2, the distribution of P_n is left-right asymmetric. In addition, to the right of the starting point ($n > S$), P_n falls sharply to be almost zero value in Fig. 2(a) because of the strong NHSE, whereas it falls softly in Figs. 2(b)–2(d). In fact, an extensive number of eigenstate are no longer localized at the left edge when the loss rates are nonuniform (3) and hence we cannot attribute the left-right asymmetry in Figs. 2(b)–2(d) directly to the NHSE. This is in stark contrast to the case considered in Ref. [41], in which the authors conclude that the NHSE is necessary for the edge burst. Below, we explore this issue in more detail.

Let us find the energy spectra for the ring and open configurations. The ring configuration is the one for which the left and right edges of the lattice are connected ($\psi_{N+1}^A = \psi_1^A$, $\psi_0^A = \psi_N^A$, $\psi_{N+1}^B = \psi_1^B$, $\psi_0^B = \psi_N^B$) and the open configuration is the one with two open edges ($\psi_0^A = \psi_{N+1}^A = \psi_0^B = \psi_{N+1}^B = 0$). The ring lattice has extra couplings between the edges than the open lattice, but this small change leads to a drastic spectral change in the case of

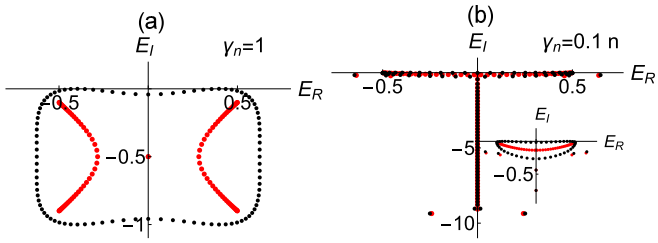

FIG. 3. The energy spectra for the (a) uniform and (b) nonuniform loss rates, where the black and red points are for the ring and open geometries, respectively. The spectra for open and ring lattices are drastically different only for the uniform lattice, indicating that NHSE occurs for the uniform one. The spectra are T shaped for the nonuniform lattice, and close the imaginary gap. In the inset, we show the spectra close to the E_R axis. The parameters are $t_1 = 0.3$, $t_2 = 0.5$, and $N = 96$.

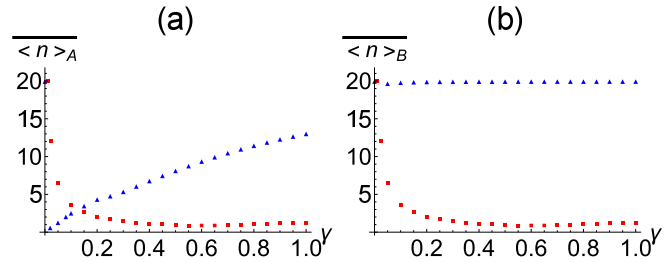

FIG. 4. The averaged mean displacements $\overline{\langle n\rangle}_A$ and $\overline{\langle n\rangle}_B$ as a function of γ for the $\mathcal{A}$ and $\mathcal{B}$ sublattices, respectively. They decrease for the open lattice with the uniform loss rates, $\gamma_n = \gamma$ (in red) indicating that NHSE occurs. However, an extensive number of eigenstate localizations do not occur at the left edge with the nonuniform loss rates, $\gamma_n = \gamma n$ (in blue), since the averaged mean displacements are not small for both sublattices. The parameters are $t_1 = 0.3$, $t_2 = 0.5$, and $N = 40$.

the uniform loss rate $\gamma_n = \gamma$, which is an indication of the NHSE [42]. The spectrum for the ring lattice makes a loop in the complex energy plane, whereas the spectrum for the open lattice is placed inside this loop [Fig. 3(a)]. Similarly, the corresponding eigenstates have different characters. An extensive number of eigenstates are localized at one edge of the open lattice, whereas the eigenstates are extended for the ring lattice. However, such a drastic spectral difference does not arise in the case of the nonuniform loss rate (3). The spectra for the ring and open lattices are T shaped [Fig. 3(b)]. The eigenvalues for the ring lattice make a tight loop along the E_R axis [inset of Fig. 3(b)], while they almost coincide with the eigenvalues for the open lattice along the E_I axis. This loop is compressed along the vertical direction as N and γ increase and becomes a line along the E_R axis for the semi-infinite boundary condition ($N \to \infty$), meaning that the spectrum perfectly becomes T shaped. We can also study the NHSE by exploring the localization character of the eigenstates for the open lattice. In order to quantify the skin localization, we use the averaged mean displacement over all energy eigenvalues for both sublattices,

$$\overline{\langle n\rangle}_{A,B} = \frac{1}{N}\sum_E \sum_n n\left|\phi_n^{A,B}\right|^2, \tag{4}$$

where $\phi_n^{A,B}$ are the normalized stationary solutions $\psi_n^A(t) = e^{-iEt}\,\phi_n^A$ and $\psi_n^B(t) = e^{-iEt}\,\phi_n^B$ with $\sum_n |\phi_n^A|^2 + |\phi_n^B|^2 = 1$. A skin state localized at the left edge makes little contribution in this summation, whereas an extended state or a state localized away from the left edge make a high contribution. Therefore, the averaged mean displacement is much smaller than N if the system is in the skin phase at which an extensive number of eigenstates are tightly localized at the left edge. We plot the averaged mean displacements as a function of γ for the uniform (in red) and nonuniform (in blue) loss rates in Fig. 4. In the case of the uniform loss rate, it decreases with γ in both sublattices since the states get localized more tightly at the left edge due to the NHSE. However, this is not the case for the nonuniform loss rate, and moreover both sublattices show different behaviors. An extensive number of eigenstates can be tightly localized at the left edge only in the $\mathcal{A}$ sublattice if γ is small. We also numerically see that eigenstates in the $\mathcal{A}$ sublattice, ϕ_n^A, become extended for large values of γ. The system as a whole is not in the skin phase since $\overline{\langle n\rangle}_B$ is nearly equal to $N/2$ at $\gamma = 0$ and this changes slightly with γ. To be more precise, the eigenstates in the $\mathcal{B}$ sublattice form a complex Wannier-Stark ladder, i.e., the system gives rise to an almost equidistantly spaced energy spectrum in the imaginary axis (the corresponding potential can be thought of as a complex electric potential, leading to Wannier-Stark localization [43]). Therefore, localization occurs around each lossy lattice point, leading to an insulating behavior in the $\mathcal{B}$ sublattice in the context of transport. Therefore the quantum walker is mostly transported in the $\mathcal{A}$ sublattice (conducting) to the left edge from which it decays. The degree of localization (de-

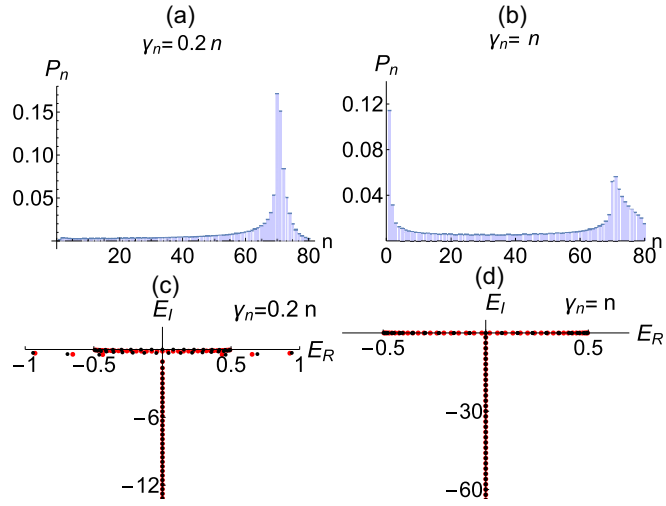

FIG. 5. P_n for two different γ_n with (a) $P_1/P_{\min} = 1$ and (b) $P_1/P_{\min} = 23$. The corresponding spectra in the complex plane have a T-shaped structure. (c), (d) The ring (in black) and open (in red) lattices have almost the same spectra. Both systems practically satisfy the imaginary gapless condition. [The maximum eigenvalues on the imaginary axis for the ring lattices are 0.009 and 0.002 for (c) and (d), respectively. These very small but nonzero values are due to the finiteness of the lattice.] The parameters are $t_1 = 0.7$, $t_2 = 0.5$, $N = 80$, and $S = 70$.

localization) in the $\mathcal{B}$ ($\mathcal{A}$) sublattice increases with γ, so the edge burst is enhanced with increasing γ, and the ratio P_1/P_S increases with γ as we numerically see in Figs. 2(b)–2(d). To this end, we think that the edge burst can be seen as long as the $\mathcal{B}$ sublattice has an insulating character. As an example, we consider random values of γ_n at which Anderson localization occurs in B sublattice and see that the edge burst can occur.

We next discuss the reason for why the left-right asymmetry of P_n appears even in the absence of NHSE. We begin to note that the $\mathcal{A}$ and $\mathcal{B}$ sublattices favor opposite propagations even in the Hermitian case ($\gamma = 0$), implying that the asymmetric behavior of P_n has nothing to do with the non-Hermiticity directly. This is because the signs of the forward and backward couplings ($it_2/2$ and $-it_2/2$) in the $\mathcal{A}$ sublattice are reversed in the $\mathcal{B}$ sublattice. This phase difference generates counterclockwise motions in the unit cell such that the $\mathcal{A}$ and $\mathcal{B}$ sublattices favor motions to the left and right, respectively. In the Hermitian lattice, the quantum walker moves to the left (right) in the $\mathcal{A}$ ($\mathcal{B}$) sublattice in such a way that no net motion is generated. Fortunately, the motion towards the right in the $\mathcal{B}$ sublattice is suppressed if we introduce losses in the B sublattice. This leads to asymmetric behavior of the quantum walker in our system. Note that this asymmetric behavior disappears if the loop in the unit cell is broken at $t_1 = 0$.

As mentioned above, the edge burst for the uniform lattice is thought to originate jointly from NHSE and the imaginary gaplessness (the spectrum under periodic boundary conditions touches the real axis and closes the imaginary gap) [41]. The T-shaped spectra in the complex plane seem to satisfy the imaginary gapless condition for the appearance of the edge bursts in our specific examples. However close inspections reveal that there may be some other examples with T-shaped spectra but without the edge burst effect. Let us choose $t_1 > t_2$. We show two such examples in Fig. 5 with T-shaped spectra. The edge burst does not appear for a small value of γ [Fig. 5(a)]. However, it appears when γ is large [Fig. 5(b)].

A relatively huge peak at the edge in the distribution of the decay probabilities in the bipartite lossy lattices is evidence of the so-called edge burst. In this Letter, we consider such lattices with the nonuniform loss rate and show that an edge burst occurs even in the absence of skin localization. We discuss that the left-right asymmetry of the decay probabilities can be due to the phase difference of the couplings in the unit cell. We also show that the edge burst may not appear even if the spectrum closes the imaginary gap in the complex energy plane. Our Letter shows interesting dynamics and can stimulate other researchers to study the dynamics of non-Hermitian systems in order to find the real source of the edge burst.

Acknowledgments. H.R. acknowledges the support by the Army Research Office Grant No. W911NF-20-1-0276, and NSF Grants No. PHY-2012172 and No. OMA-2231387.

[1] S. Yao, F. Song, and Z. Wang, Non-Hermitian Chern Bands, Phys. Rev. Lett. **121**, 136802 (2018).
[2] S. Yao and Z. Wang, Edge States and Topological Invariants of Non-Hermitian Systems, Phys. Rev. Lett. **121**, 086803 (2018).
[3] H. Jiang, L.-J. Lang, C. Yang, S.-L. Zhu, and S. Chen, Interplay of non-Hermitian skin effects and Anderson localization in nonreciprocal quasiperiodic lattices, Phys. Rev. B **100**, 054301 (2019).
[4] C. Yuce, Anomalous features of non-Hermitian topological states, Ann. Phys. **415**, 168098 (2020).
[5] Y. Liu, Q. Zhou, and S. Chen, Localization transition, spectrum structure, and winding numbers for one-dimensional non-Hermitian quasicrystals, Phys. Rev. B **104**, 024201 (2021).
[6] C. Yuce, $\mathcal{PT}$ symmetric Aubry-Andre model, Phys. Lett. A **378**, 2024 (2014).
[7] J. Claes and T. L. Hughes, Skin effect and winding number in disordered non-Hermitian systems, Phys. Rev. B **103**, L140201 (2021).
[8] L.-Z. Tang, G.-Q. Zhang, L.-F. Zhang, and D.-W. Zhang, Localization and topological transitions in non-Hermitian quasiperiodic lattices, Phys. Rev. A **103**, 033325 (2021).
[9] Q.-B. Zeng and Y. Xu, Winding numbers and generalized mobility edges in non-Hermitian systems, Phys. Rev. Res. **2**, 033052 (2020).
[10] C. Yuce, Nonlinear non-Hermitian skin effect, Phys. Lett. A **408**, 127484 (2021).
[11] Y. Yi and Z. Yang, Non-Hermitian Skin Modes Induced by On-Site Dissipations and Chiral Tunneling Effect, Phys. Rev. Lett. **125**, 186802 (2020).
[12] S. Longhi, Topological Phase Transition in non-Hermitian Quasicrystals, Phys. Rev. Lett. **122**, 237601 (2019).
[13] S. Schiffer, X.-J. Liu, H. Hu, and J. Wang, Anderson localization transition in a robust $\mathcal{PT}$-symmetric phase of a generalized Aubry-André model, Phys. Rev. A **103**, L011302 (2021).
[14] Z. Ozcakmakli Turker and C. Yuce, Open and closed boundaries in non-Hermitian topological systems, Phys. Rev. A **99**, 022127 (2019).
[15] C. Yuce, Non-Hermitian anomalous skin effect, Phys. Lett. A **384**, 126094 (2020).
[16] X. Cai, Boundary-dependent self-dualities, winding numbers, and asymmetrical localization in non-Hermitian aperiodic one-dimensional models, Phys. Rev. B **103**, 014201 (2021).
[17] C. H. Lee and R. Thomale, Anatomy of skin modes and topology in non-Hermitian systems, Phys. Rev. B **99**, 201103(R) (2019).
[18] P. Wang, L. Jin, and Z. Song, Non-Hermitian phase transition and eigenstate localization induced by asymmetric coupling, Phys. Rev. A **99**, 062112 (2019).
[19] M. Ezawa, Non-Hermitian boundary and interface states in nonreciprocal higher-order topological metals and electrical circuits, Phys. Rev. B **99**, 121411(R) (2019).
[20] C. H. Lee, L. Li, and J. Gong, Hybrid Higher-Order Skin-Topological Modes in Nonreciprocal Systems, Phys. Rev. Lett. **123**, 016805 (2019).
[21] L. Li, C. H. Lee, S. Mu, and J. Gong, Critical non-Hermitian skin effect, Nat. Commun. **11**, 5491 (2020).
[22] F. K. Kunst, G. V. Miert, and E. J. Bergholtz, Extended Bloch theorem for topological lattice models with open boundaries, Phys. Rev. B **99**, 085427 (2019).

[23] C. Yuce and H. Ramezani, Coexistence of extended and localized states in one-dimensional non-Hermitian Anderson model, Phys. Rev. B **106**, 024202 (2022).
[24] H. Jiang, R. Lü, and S. Chen, Topological invariants, zero mode edge states and finite size effect for a generalized non-reciprocal Su-Schrieffer-Heeger model, Eur. Phys. J. B **93**, 125 (2020).
[25] C. Yuce and H. Ramezani, Robust Exceptional Points in Disordered Systems, Europhys. Lett. **126**, 17002 (2019).
[26] J. Y. Lee, J. Ahn, H. Zhou, and A. Vishwanath, Topological Correspondence between Hermitian and Non-Hermitian Systems: Anomalous Dynamics, Phys. Rev. Lett. **123**, 206404 (2019).
[27] Y. Cao, Y. Li, and X. Yang, Non-Hermitian bulk-boundary correspondence in a periodically driven system, Phys. Rev. B **103**, 075126 (2021).
[28] C. Yuce, Quasi-stationary solutions in 1D non-Hermitian systems, Phys. Lett. A **403**, 127384 (2021).
[29] C. Yuce, Spontaneous topological pumping in non-Hermitian systems, Phys. Rev. A **99**, 032109 (2019).
[30] J. Zhong, K. Wang, Y. Park, V. Asadchy, C. C. Wojcik, A. Dutt, and S. Fan, Nontrivial point-gap topology and non-Hermitian skin effect in photonic crystals, Phys. Rev. B **104**, 125416 (2021).
[31] K.-I. Imura and Y. Takane, Generalized bulk-edge correspondence for non-Hermitian topological systems, Phys. Rev. B **100**, 165430 (2019).
[32] K. Yokomizo and S. Murakami, Non-Bloch Band Theory of Non-Hermitian Systems, Phys. Rev. Lett. **123**, 066404 (2019).
[33] H. Shen, B. Zhen, and L. Fu, Topological Band Theory for Non-Hermitian Hamiltonians, Phys. Rev. Lett. **120**, 146402 (2018).
[34] N. Okuma, K. Kawabata, K. Shiozaki, and M. Sato, Topological Origin of Non-Hermitian Skin Effects, Phys. Rev. Lett. **124**, 086801 (2020).
[35] K. Zhang, Z. Yang, and C. Fang, Correspondence between Winding Numbers and Skin Modes in Non-Hermitian Systems, Phys. Rev. Lett. **125**, 126402 (2020).
[36] D. S. Borgnia, A. J. Kruchkov, and R.-J. Slager, Non-Hermitian Boundary Modes and Topology, Phys. Rev. Lett. **124**, 056802 (2020).
[37] Z. Yang, K. Zhang, C. Fang, and J. Hu, Non-Hermitian Bulk-Boundary Correspondence and Auxiliary Generalized Brillouin Zone Theory, Phys. Rev. Lett. **125**, 226402 (2020).
[38] K. Wang, A. Dutt, K. Y. Yang, C. C. Wojcik, J. Vuckovic, and S. Fan, Generating arbitrary topological windings of a non-Hermitian band, Science **371**, 1240 (2021).
[39] L. Xiao *et al.*, Observation of topological edge states in parity-time-symmetric quantum walks, Nat. Phys. **13**, 1117 (2017).
[40] L. Wang, Q. Liu, and Y. Zhang, Quantum dynamics on a lossy non-Hermitian lattice, Chin. Phys. B **30**, 020506 (2021).
[41] W.-T. Xue, Y.-M. Hu, F. Song, and Z. Wang, Non-Hermitian Edge Burst, Phys. Rev. Lett. **128**, 120401 (2022).
[42] Z. Gong, Y. Ashida, K. Kawabata, K. Takasan, S. Higashikawa, and M. Ueda, Topological Phases of Non-Hermitian Systems, Phys. Rev. X **8**, 031079 (2018).
[43] M. Glück, A. R. Kolovsky, and H. J. Korsch, Wannier-Stark resonances in optical and semiconductor superlattices, Phys. Rep. **366**, 103 (2002).